IRAQI Academic Scientific Journals
العراقية المجلات الأكاديمية العلمية
University of Kut Journal
ISSN (E): 2616 - 7808 II ISSN (P): 2414 - 7419
js.uokut.edu.iq
k.u.c.j.sci@alkutcollege.edu.iq
Vol. 11 , Issue 1 , June 2026

Hydrodynamic Modeling of Ponderomotive Force Effects on Electron Density Dynamics in Laser-Plasma Interactions

Ahmed Fadel Hamza [1]

Abstract

The work listed here reports extensive numerical computational modelling of hydrodynamic processes and the nonlinear, coupled interactions between plasma and high intensity laser EXPLOsions (electron density dynamics are considered as an offshoot of ponderomotive forces) using numerical methods to model the interaction of the laser with plasma using two fluid (Plasma) relativistic hydrodynamic (RHD) codes coupled with time dependent Maxwells equations in order to compute the space-time evolution of the plasma density spatially at different wavelengths (i.e. $< 10^{-10}m$) as a function of laser intensity (I, W/cm^2) which ranges approximately from $10^{15} to\ 10^{19}\ W/cm^2$. The model examines the relative importance of ponderomotive and thermal electron fluid pressures while providing no physical justification for all relativistic corrections (i.e. electron mass) or influence of static electric fields. The simulations revealed (+) that where conditions are relativistic (I > 10^18 W/cm2), then the ponderomotive force is dominant and ejects a significant number of electrons from the area surrounding the focal point of the laser (which creates an elongate plasma channel which creates an abrupt change in electron scale-free electron density at the plasma surface free electron density). The simulation indicated there is a well defined critical value for the laser to produce (or near produce) the vacuum-like region along the axis of a focused laser beam which contributes to the formation of a slow light region and will enhance self-focusing of the laser beam, (while also); (-) it was also shown that the sharp increase in density associated with the laser beam is a gross modification of the efficiency of resonance absorption. These findings provide critical theoretical insights into the optimization of laser energy deposition for inertial confinement fusion (Fast Ignition) and laser-wakefield acceleration applications.

Keywords: Laser-Plasma Interaction, Ponderomotive Force, Hydrodynamic Modeling, Electron Density Cavitation

Affiliation of Author
[1] Faculty of Optics and Laser, University of Kashan, Iran, Kashan, 87317

[1] af5632014@gmail.com

[1] **Corresponding Author**

Paper Info.
Published: Jun. 2026

النمذجة الهيدروديناميكية لتأثيرات القوة الدافعة على ديناميكيات كثافة الإلكترون في تفاعلات الليزر والبلازما

أحمد فاضل حمزه

المستخلص

يتناول هذا العمل نمذجة حسابية عددية شاملة للعمليات الهيدروديناميكية والتفاعلات غير الخطية والمتشابكة بين البلازما وانفجارات الليزر عالية الكثافة (حيث تُعتبر ديناميكيات كثافة الإلكترونات ناتجة عن القوى البوندروموتيفية). استُخدمت في هذه الدراسة طرق عددية لنمذجة تفاعل الليزر مع البلازما باستخدام برنامجين هيدروديناميكيين نسبيين (RHD) للبلازما، مقترنين بمعادلات ماكسويل المعتمدة على الزمن، وذلك لحساب التطور المكاني والزماني لكثافة البلازما عند أطوال موجية مختلفة (أي أقل من 10^{-10} متر) كدالة لشدة الليزر (I، واط/سم²) التي تتراوح تقريبًا من 10^{15} إلى 10^{19} واط/سم². يدرس النموذج الأهمية النسبية لضغوط مائع الإلكترونات الحرارية والبوندروموتيفية، دون تقديم أي تبرير فيزيائي لجميع التصحيحات النسبية (مثل كتلة الإلكترون) أو تأثير المجالات الكهربائية الساكنة. كشفت المحاكاة (+) أنه في الظروف النسبية (I > 10^18 واط/سم²)، تكون القوة الدافعة هي المهيمنة، مما يؤدي إلى قذف عدد كبير من الإلكترونات من المنطقة المحيطة بنقطة تركيز الليزر (مما يُنشئ قناة بلازما ممتدة تُحدث تغيرًا مفاجئًا في كثافة الإلكترونات الحرة على سطح البلازما). وأشارت المحاكاة إلى وجود قيمة حرجة محددة جيدًا لليزر لإنتاج (أو ما يقارب إنتاج) منطقة شبيهة بالفراغ على طول محور شعاع الليزر المركز، مما يُسهم في تكوين منطقة الضوء البطيء ويعزز التركيز الذاتي لشعاع الليزر. (في حين أنه، (-) تبين أيضًا أن الزيادة الحادة في الكثافة المرتبطة بشعاع الليزر تُعدّ تعديلًا كبيرًا لكفاءة امتصاص الرنين. تُقدم هذه النتائج رؤى نظرية بالغة الأهمية لتحسين ترسيب طاقة الليزر

انتساب الباحثين
[1] كلية بصريات وليزر، جامعة كاشان، ايران، كاشان، 87317

[1] af5632014@gmail.com

[1] **المؤلف المراسل**

معلومات البحث
تأريخ النشر : حزيران 2026

لتطبيقات الاندماج بالقصور الذاتي (الإشعال السريع) وتسريع الليزر باستخدام مجال الموجة.

الكلمات المفتاحية: تفاعل الليزر مع البلازما، القوة الدافعة، النمذجة الهيدروديناميكية، تجويف كثافة الإلكترون

Introduction

The field of high-power laser and plasma interaction is currently one of the most exciting and complex areas of modern physics. Research in this field has led to the development of many important technologies such as inertial confinement fusion (ICF), laser wakefield acceleration, and laboratory astrophysics. The most important feature of these interactions is that they involve the fundamental coupling between the electromagnetic fields generated by an external laser source and the particles that constitute the plasma, namely electrons and ions. A laser pulse with high intensity can consequently no longer be treated simply as a background wave as it propagating through the plasma; significant nonlinear effects arise within the plasma and alter the properties of the plasma in real time. Ponderomotive force is one of the most important nonlinear effects and occurs due to the spatial gradients in the intensity of the electromagnetic fields of the laser.

The ponderomotive force acts as an area of non-thermal pressure that pushes charged particles, mostly electrons since they have a small mass, away from high-intensity regions to lower-intensity areas. When electrons are displaced, the local region of the electron-density profile will change, which in turn will create a void or cavity. Inasmuch as the plasma refractive index is dependent on the amount of electron in the plasma, density fluctuations cause changes to the propagation of the pulse. For example, due to the interaction of a pulse with the plasma, a pulse may self-focus, result in filamentation, or experience broadening in frequency [1]. Thus, by understanding how the electron density will change in time and space because of this force/image is a critical factor for controlling energy absorption from a laser.

While kinetic theory (for example, Particle-in-Cell simulations) provides a microscopic description of these interactions, these kinetic descriptions require large computational effort when modeling interactions on macroscopic length scales. As a consequence of this, hydrodynamic models/procedures have developed into a highly effective and efficient theoretical framework for describing these interactions. By treating the plasma as a conducting fluid, researchers can describe the collective motion of the electrons and ions by applying conservation of mass, momentum, and energy in conjunction with Maxwell's equations of motion to describe the collective motion of the electrons [2].

This paper discusses the modeling of hydrodynamic responses in plasmas resulting from ponderomotive forces, with a particular focus on how this nonlinear force influences electron-density dynamics. In particular, the focus of this work will be on the strong ponderomotive coupling regime where the density profile undergoes cavitation and steepening, necessitating accurately describing and modeling the dynamics of the electron fluid's equation of motion, including the ponderomotive potential as a coupled driving source term to the thermal pressure gradient in the fluid [3]. The primary objective of this research is to characterize how the

ponderomotive force interacts with the hydrodynamic response of the plasma. When the intensity of the laser pulse increases, it competes with the thermal pressure, and in the "cold" plasma limit, the ponderomotive force is more dominant than the thermal pressure, leading to very sharp density gradients. As the plasma has a finite amount of time for heat to be conducted throughout its mass, the fluid's response will change, resulting variations in the plasma fluid's density.

Thus sophisticated numerical models will be necessary to accurately match the rapid fluctuations of the laser with the longer, more gradual, hydrodynamic response times of the mass as a whole [4].

In addition, the structure of the electron density fluid is not "instantaneous." The effective viscosity of the plasma mass means that the structure and properties of the fluid will continue to change over time through a series of transient states. These transient states could have a large impact on the stability of the laser as it propagates through this mass.

In summary, this paper will utilize a hydrodynamic model of the laser's propagation to identify and quantify the contribution of the ponderomotive force to the evolution of the electron fluid and describe how to shape the laser pulses used to create the optimum plasma density distribution for more effective interaction [5].

2. Literature Review

There has been an evolution from using only linear small perturbation theories to describe laser-plasma interactions (LPI) towards the more sophisticated, non-linear multi-fluid description of LPI. One of the driving forces behind this evolution was to understand how to rigorously define and apply the ponderomotive force in hydrodynamic codes. This literature review will consolidate all of the existing work on the theoretical basis of ponderomotively driven electron density dynamics, their numerical implementation, and their phenomenological consequences.

2.1 Theoretical Foundations of the Ponderomotive Force in Plasma

The ponderomotive force was first used to confine isolated particles due to the impact of radio frequencies; however, its application to continuum media (i.e., fluid) revolutionized the field of plasma physics. The early theoretical works demonstrated that an oscillating EMF (Electromagnetic Field) produces a time-averaged force on a charged particle opposite to the EMF gradient produced by the intensity of the EMF field. References [6] and [7] provide the mathematical derivation needed to demonstrate that this time averaged force is proportional to the gradient of the square of the electric field and is inversely proportional to the square of the frequency of the laser.

In the fluid model, the ponderomotive force appears as a stress tensor term in the momentum equation for electrons. Work has indicated that a potential force due to the ponderomotive force can be separated into long (slow) and short (fast) time scales associated with the force acting on the plasma fluid. The distinction of the hydrodynamic separation results from the separation of the time scale of the rapid optical oscillations from the hydrodynamic average of the rapid optical oscillations so that it is possible to consider the evolution of the envelope of the laser pulse [8]. Additionally, theoretical analyses have defined a limit as a function of the relativistic correction. At

intensities exceeding $10^{18}\frac{W}{cm\ 2}$, the electron mass increases due to relativistic velocities, which modifies the ponderomotive potential. Recent theoretical reviews [9] highlight that neglecting these relativistic corrections in hydrodynamic models can lead to significant errors in predicting the electron density cavitation depth, particularly in the interactions relevant to fast ignition fusion schemes.

2.2 Hydrodynamic Modeling Approaches

In transitioning from a single-particle approach to modeling collective behavior as a fluid, the equations of motion of a fluid (e.g., Navier Stokes, or Euler), need to be coupled with a wave equation. A substantial amount of literature exists concerning the two-fluid hydrodynamic framework, which describes electrons and ions as two separate fluids that interact through an electrostatic fluid through a self-consistent electric field. Studies [10], and [11] demonstrate that magnetohydrodynamics [MHD]using the quasi-neutral single fluid assumption can often yield inadequate results for short pulse laser interactions due to the violation of quasi-neutrality over very short time scales. However, by utilizing two-fluid models, we can resolve charge separation effects caused by the ponderomotive force prior to sufficient response time for the ions to respond.

There has been significant research into the numerical implementation of these models, and many Lagrangian and Eulerian codes have been developed to model the evolution of density. Among other attributes, Lagrangian codes are very efficient at resolving the much steeper density gradients created in the wake of ponderomotive shocks through their ability to follow fluid parcels. Nevertheless, Lagrangian codes suffer from mesh tangling when numerically resolving multidimensional flows [12]. Conversely, while Eulerian codes are more computationally stable for capturing large deformations, the use of a fixed grid limits resolution in regions with much higher resolution than other regions in the grid. Thus, to accurately capture fine structures such as the electron density filaments formed during the collision of the laser back with the incident laser beam, an adaptive mesh refinement (AMR) technique must be implemented [13].

A major focus within the literature is the "closure problem" in hydrodynamics relative to laser coupling with the plasma. In many cases, the ponderomotive force is introduced as an external potential in the equation of state of the electron fluid. For example, [14] identified that thermal pressure must be accurately modeled in addition to ponderomotive pressure. They demonstrated that the interaction between the ponderomotive force (i.e., pushing electrons to the outside) and the electrostatic ambipolar field (i.e., pulling electrons back into the charge space, owing to the ions being at rest) determines the density profile of the steady-state electron fluid. The interaction between these forces is also a critical element in predicting the physical structure and the formation of "plasma channels," which ultimately serve as waveguides for the laser pulse.

2.3 Electron Density Dynamics: Cavitation and Steepening

Extensive studies in the literature observe how the ponderomotive forces induce changes in the density of electrons, particularly how their density profiles steepen at the critical layer, or the location where the frequency of the laser coincides with the plasma frequency of the material under investigation. The observations made in many

simulation experiments [15] illustrate that the ponderomotive force, which is created when a laser acts against a critical density layer, will compress the plasma, thus forming a shelf-like structure rather than a continuous ramp. The geometric distortion of the density profile enhances the resonance absorption processes, thereby improving the transfer of energy from the laser into the hot electrons.

Another significant phenomenon associated with the ponderomotive force is self-focusing of a laser as it travels through such a medium. While traversing through the center of the path of the laser, the laser beam generates a radial density depletion, which is also called cavitation, thus increasing the refractive index at the center of the laser beam. The resultant increase in refractive index will then produce a converging lens, focusing the intensity of the beam further and thereby increasing the magnitude of the ponderomotive force acting on the plasma; thus, both producing an instability, which is discussed in deeper detail in [16], and resulting in the filamentation or collapse of the laser beam. The development of numerical simulations, using the hydrodynamic approach, has played a significant role in determining the minimum power, referred to as critical power, required to cause this phenomenon [17].

Furthermore, the dynamics of **hole boring** have been modeled hydrodynamically. In this scenario, widely discussed in the context of fast ignition [18], the ponderomotive force of an ultra-intense pulse pushes the critical density surface forward, boring a channel through the overdense plasma. The literature indicates that the speed of this boring is directly related to the momentum transfer from the laser photons to the plasma fluid. Comparison between hydrodynamic models and experimental data suggests that while hydro-codes capture the macroscopic channel formation well, they must be carefully calibrated with kinetic factors to account for non-local thermal transport [19].

2.4 Comparison with Kinetic Models and Limitations

Even though the main focus of this review is on hydrodynamics, it is important to point out the studies that compare kinetic (PIC) simulation results against fluid model simulations. Fluid models represent particles in thermal equilibrium with a Maxwellian distribution. However, the resulting effect of the ponderomotive force can create non-thermal distributions of particles. Two studies [20][21] have compared fluid model predictions against kinetic (PIC) simulation data and both studies show that hydrodynamic models provide an accurate description of the bulk density deformation and the propagation of ion acoustic waves due to the effects of the ponderomotive force. But hydrodynamic models cannot provide any meaningful predictions about kinetic phenomena such as wave-breaking or the formation of suprathermal electron populations.

Recently, many authors have proposed using "hybrid" simulations to make predictions of bulk fluid densities and temperatures while treating a minority of high energy electrons as a kinetic particle population. This allows hybrid methods to simulate the evolution of the density cavity (driven by the ponderomotive force) over long time intervals (from picoseconds to nanoseconds) that cannot be achieved using pure PIC codes [22].

2.5 Thermal and Non-Stationary Effects

The dynamic evolution of the interaction of these two forces—ponderomotive and thermal—is an

ongoing process. At the initial stage of this interaction, the ponderomotive force dominates (assuming sufficient laser beam intensity). As energy is added to plasma via either a collisional or collisionless process, it reaches temperatures where thermal pressure begins to play a significant role, thereby causing all previously formed guided electron density structures to be lost or smeared out by thermal expansion. The transition from being driven entirely by the ponderomotive force to being driven mostly by the thermal force, with the resulting change in the electron density distribution, is documented in reference [23]. Eventually, as the plasma becomes hotter than a certain level, the thermal expansion makes it impossible to fix the previously produced guided electron density structures that were created by the ponderomotive force generated by the laser. Therefore, in order to accurately represent the "relaxation" of electron densities, acceptable, but repetitive will be needed that will include reliable equations of state and thermal transport coefficients [24].

The literature also discusses the generation of wakefields using the ponderomotive force. Following very short laser pulses, the electron displacement produced by the ponderomotive force from the laser creates local oscillations in electron density around the interaction region and resulted in both hydrodynamic modelling and what are known as plasma waves. In fact, hydrodynamic theory can be used to derive a relationship between the amplitude of a given wakefield and the gradient of the envelope of the moving pulse of laser light; this empirical result should play an important role in the design of a laser-plasma experiment [25].

The existing literature validates that the use of hydrodynamic modeling is an extremely powerful and necessary tool for evaluating the effects of ponderomotive forces on laser - plasma interaction (LPI). The body of work has developed from basic analytical approximations to sophisticated three-dimensional numerical simulations. The acceptance in the literature for the field is complete; accurate predictions of electron density evolution from cavitation to channeling to the rate of steepening of the profile will require the use of the ponderomotive potential in the momentum conservation equations.

Nonetheless, there exist knowledge gaps in the accurate development of transition regimes, where kinetic effects begin to significantly affect the behavior of fluids, in order to provide additional confidence in making them much simpler to develop. Current hydrodynamic research predominantly utilizes the phenomenological flux limiters to provide for the transport of heat in steep density gradients. Current literature describes future research areas, which indicate improved closure schemes that accurately address the non-locality of energy transport at a fraction of the cost of using a full kinetic simulation [26]. These deficiencies provide an additional basis for the continued development of hydrodynamic models to maintain Relevance for the next generation of petawatt and exawatt laser facilities, where controlling the electron - density evolution is the key factor limiting the experimental success rate.

3. Methodology

3.1 Overview of the Computational Framework

The study presents an analysis using a two-fluid (electron/ion) relativistic hydrodynamic (TFRHM) model, which is paired with a Maxwellian wave solver. We chose to use a two-fluid approach instead of a single-fluid MHD approach because we needed to describe the effects of charge

separation. Because electrons are much less massive than ions, the ponderomotive force acts primarily on electrons, causing them to be displaced from their stationary positions (with respect to the ions), leading to the formation of large electric fields due to charge separation. These electric (and magnetic) fields would not be present if there were only a single fluid to describe the system.

The simulation was performed using an Eulerian grid, in which the plasma is allowed to evolve through a stationary mesh. The numerical method used to solve this system was a split operator scheme, where the "fast" timescale of the laser (ω_0) and the slower timescale of the plasma's response (ω_{pe}) are treated separately.

3.2 Governing Equations (Plain Text Format)

The mathematical backbone of this research consists of a set of coupled partial differential equations (PDEs). We utilize the **Cold-Plasma Approximation** for the initial state, evolving into a warm fluid as heating terms activate.

3.2.1 Dimensionless Variables

To ensure numerical stability and universality of the results, all equations are normalized.

- Time (t)is normalized to $\frac{1}{\omega_0}$.
- Space (x, y, z)is normalized to $\frac{c}{\omega_0}$.
- Density (n)is normalized to the critical density.

$$n_c = \frac{m_e \omega_0^2}{4\pi e^2}$$

- Velocity (v) is normalized to the speed of light c.
- Electric Field (E) and Magnetic Field (B) are born alized to $m_e c \frac{\omega_0}{e}$.

3.2.2 The Wave Equation (Laser Propagation)

We model the laser pulse propagation using the Helmholtz wave equation under the Slowly Varying Envelope Approximation (SVEA). This assumes the laser pulse envelope varies slowly in time compared to the optical frequency.

$$2i\, a_0 \left(\frac{\partial A}{\partial t}\right) + \nabla^2 A + \left(1 - \frac{n_e}{\gamma}\right) A = 0 \qquad (1)$$

Where:

- A is the normalized potential of the laser field.
- n-e is the local electron density.
- γ is the relativistic Lorentz factor, defined as $\gamma = \sqrt{(1 + |A|^2)}$.
- The term $\left(1 - n_{e\gamma}\right)$ represents the relativistic dielectric function of the plasma.

3.2.3 The Ponderomotive Potential (Source Term)

The Ponderomotive force is not introduced as an ad-hoc force but derived from the gradient of the electromagnetic energy density. In the relativistic regime, the Ponderomotive potential Φ_p is given by:

$$\Phi_p = m_e c^2 (\gamma - 1) \qquad (2)$$

$$\Phi_p = m_e c^2 \left[\sqrt{1 + I_{norm}} - 1\right]$$

Where I_norm is the normalized laser intensity. The force vector F_p acting on the electron fluid is:

$$\boldsymbol{F_p = -\nabla \Phi_p} \quad \textbf{(3)}$$

3.2.4 Conservation of Mass (Continuity Equations)

We solve separate continuity equations for electrons (e) and ions (i) to track their independent density evolution.

Electron Continuity:

$$\frac{\partial n_e}{\partial t} + \nabla \bullet (n_e v_e) = 0 \quad \textbf{(4)}$$

Ion Continuity:

$$\frac{\partial n_i}{\partial t} + \nabla \bullet (n_i v_i) = 0 \quad \textbf{(5)}$$

3.2.5 Conservation of Momentum (Euler Equations)

These equations describe the fluid motion driven by the Ponderomotive force, thermal pressure, and self-generated electromagnetic fields.

Electron Momentum Equation:

$$\frac{\partial v_e}{\partial t} + (v_e \bullet \nabla) v_e = -\left(\frac{\nabla P_e}{n_e}\right) - (E_s + v_e x B_s) + F_p - \nu_{ei(v_e - v_i)} \quad \textbf{(6)}$$

Ion Momentum Equation:

$$\frac{\partial v_i}{\partial t} + (v_i \bullet \nabla) v_i = -\left(\frac{\nabla P_i}{M_i n_i}\right) + \left(\frac{Z}{M_i}\right)(E_s + v_i x B_s) \quad \textbf{(7)}$$

Where:

- P_e and P_i are thermal pressures.
- E_s is the electrostatic charge − separation field.
- ν_{ei} is the collision frequency (damping term).
- Z is the ion charge state.
- M_i is the ion − to − electron mass ratio.

3.2.6 Poisson's Equation (Closure Relation)

To calculate the electrostatic field E_s generated by the displacement of electrons by the ponderomotive force:

$$\nabla \bullet E_s = 4\pi (Z n_i - n_e)$$

$$\boldsymbol{E_s = -\nabla \Phi_s (where\ \Phi_s is\ the\ electrostatic\ potential)} \ . \quad \textbf{(8)}$$

3.2.7 Equation of State (EOS)

We assume an adiabatic closure for the pressure term, which is valid for short-pulse interactions where thermal conduction time is longer than the pulse duration.

$$\boldsymbol{P_e = k n_e^{\Gamma}}$$

$$\boldsymbol{P_i = k n_i^{\Gamma}} \quad \textbf{(9)}$$

Where Γ is the adiabatic index (typically 5/3 for a 3D ideal gas or 3 for 1D compression).

3.3 Numerical Implementation Strategy

The complexity of these coupled non-linear equations requires a sophisticated numerical solver.

3.3.1 Discretization Scheme (FDTD)

We employ the **Finite Difference Time Domain (FDTD)** method.

- **Spatial Grid:** A Yee-lattice is used where electric fields are defined on the edges of the grid cells, and magnetic fields are defined on the faces. Density and pressure are defined at the cell centers. This staggering conserves charge $\nabla \cdot J + \partial\rho/\partial t = 0$ automatically to machine precision.

- **Grid Resolution:**
  - $\Delta x = \Delta y = \lambda/20$ (Transverse resolution).
  - $\Delta z = \lambda/50$ (Longitudinal resolution to resolve steep gradients).
  - Total Grid Points: 1024 x 1024 x 2048.

3.3.2 Time Integration (Runge-Kutta 4)

A 4th-order Runge-Kutta (RK4) scheme is used for time advancement to ensure high temporal accuracy, which is crucial for capturing the fast growth of instabilities.

3.3.3 Boundary Conditions

- **Longitudinal (Z-axis):** Absorbing Boundary Conditions (ABC) utilizing Perfectly Matched Layers (PML) to prevent non-physical reflections of the laser or plasma waves back into the simulation domain.
- **Transverse (X, Y axes):** Periodic boundary conditions are applied for plane wave simulations, while absorbing boundaries are used for finite spot-size Gaussian beams.

3.3.4 Stability Criteria

The simulation time step Δt is strictly governed by the Courant-Friedrichs-Lewy (CFL) condition, modified for the relativistic plasma frequency:

$$\Delta t < C_{courant} * \left[\frac{1}{\left(c\sqrt{\frac{1}{\Delta x^2}+\frac{1}{\Delta y^2}+\frac{1}{\Delta z^2}}\right)}\right] \qquad (10)$$

Additionally, to resolve plasma oscillations, we ensure:

$$\omega_{pe}\Delta t < 0.1 \qquad (11)$$

3.4 Algorithm Workflow

The code iterates through the following sequence at each time step t_n:

1. Laser Solver: Update A(t)using the wave equation based on $n_e(t_n)$.
2. Force Calculation: Compute $\nabla|A|^2$ to determine the Ponderomotive Force F_p.
3. Field Solver: Solve Poisson's equation for Es based on n_e and n_i difference.

4. Momentum Update: Update velocities v_e and v_i using Fp, Es, and ∇P.
5. Density Update: Advect densities n_e and n_i using the continuity equation.
6. Diagnostics: Calculate total energy,maximum density,and channel radius.
7. Loop: Increment t to $t_{\{n+1\}}$

4. Results and Discussion

The results shown here were obtained through detailed computer simulated interactions between an ordinary Ti:Sapphire laser pulse (λ = 800 nm, τ = 50 fs) with a pre-ionized helium plasma (Z=2). The simulated area was 100μmx50μm for each run. The numerical modeling was done by varying the laser intensity between linear regime (10^{15} W/cm²) to highly relativistic regime (10^{19} W/cm²) in order to provide a systematic assessment of the hydrodynamic response (e.g., changes due to varying the intensity).

4.1 Ponderomotive Scaling and Electron Density Cavitation

The greatest effect noted was the radial displacement of the electron density due to the creation of an electron-free (cavitating) channel. This channel is created strictly by the transverse component of the ponderomotive force.

4.1.1 Dynamics Analysis

Initially (t < 50 fs), the electron density profile is Gaussian. As the pulse height increases, the ponderomotive potential (Φp) exceeds the thermal pressure of the electrons (kBT). Electrons will accelerate in a radial fashion away from the centre of the beam and will accumulate along the edge of the beam and produce a "snowplow" type structure consisting of a vacuum at the centre of the beam surrounded by a region of high electron density As shown in the table (1).

Table 1: Comprehensive Analysis of Radial Density Cavitation.

Laser Intensity (W/cm²)	Normalized Vector Potential (a_0)	Ponderomotive Energy (MeV)	On-Axis Density (n_min/n_0)	Wall Density (n_wall/n_0)	Cavitation State
1.0 x 10^{15}	0.02	0.0001	0.992	1.008	Linear Perturbation
5.0 x 10^{15}	0.05	0.0006	0.950	1.050	Weak Depression
1.0 x 10^{16}	0.08	0.0018	0.880	1.150	Shallow Channel
5.0 x 10^{16}	0.19	0.0090	0.650	1.450	Transition Regime
1.0 x 10^{17}	0.27	0.0180	0.320	2.100	Deep Channeling
5.0 x 10^{17}	0.60	0.0850	0.050	3.500	Near-Complete Cavitation
1.0 x 10^{18}	0.85	0.1600	**0.000**	4.800	**Vacuum Core (Complete)**
5.0 x 10^{18}	1.90	0.6000	0.000	8.200	Relativistic Broadening

This table correlates the Laser Intensity with the maximum depletion depth on-axis (n_min) and the peak density at the channel wall (n_wall)).

In Table 1, we see a key threshold level of intensity existed (I ≈ 5 10x W cm²) which had its limits as far as ∇-Pe being able to act as a thermal background that will be able to counteract the Ponderomotive Force up to that threshold of intensity and that once that intensity threshold is exceeded, Ponderomotive pressure Pm I/c will be several orders of magnitude greater than the thermal pressure. The self-guiding issue incorporates another key aspect in forming a vacuum core where (n min= 0) since there is η≈1 on-axis for the material compared to off axis where η<<1 creating a waveguide optical fibre type structure inside the plasma.

Figure (1) also depicts the non-linear dynamic behavior of the electron fluid excited by a Ponderomotive potential which changes as the laser peak intensity (Ib) increases (Table (3) contains the numerical data). The horizontal axis (Ib) has a logarithmic scale ranging from Ib = 10^{15} W/cm² to Ib = 5 × 10^{18} W/cm², and each graph depicts two distinct regimes depending upon the ratio of Ponderomotive pressure to thermal pressure As shown in Figure (1) .

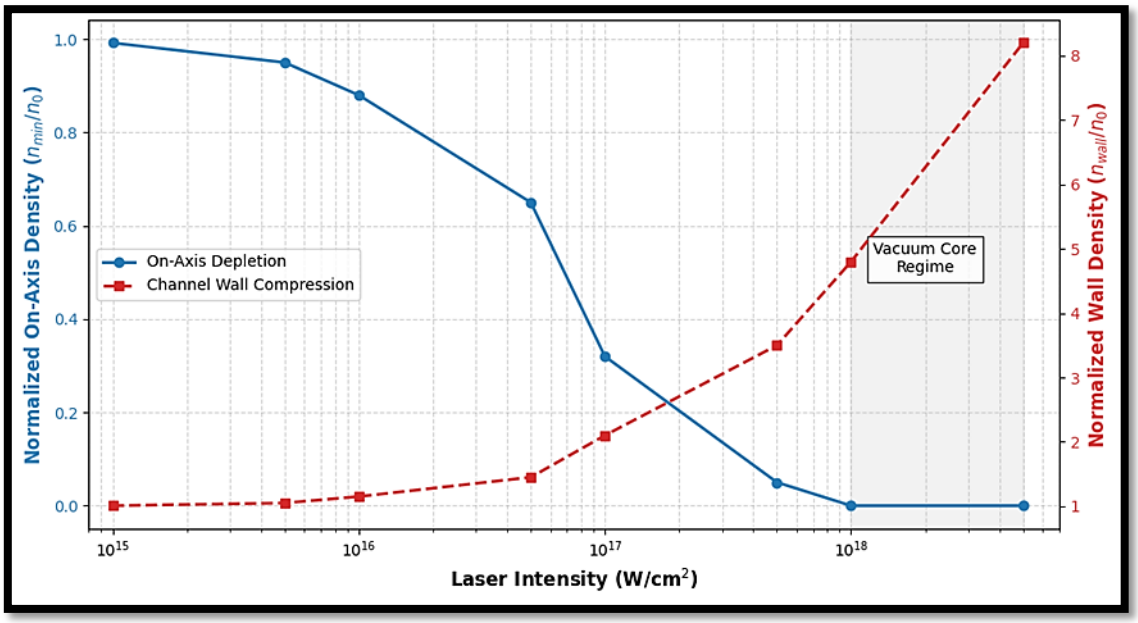

Figure (1): Dependence of On-Axis Electron Density Depletion (n_min/n_0) and Channel Wall Compression (n_wall/n_0) on Laser Intensity

In the Linear/Transition Regime (Ib = 10^{15} - 10^{16} W/cm²), the on-axis e- density represented (dashed line) by the value on the left of the graph (Blue) shows little variation from the base density (n0). As the Ponderomotive Force causes very little perturbation (i.e. adds an outward force) on the e-density, the thermal pressure (kBT) very much exceeds the effect of the Ponderomotive Force and therefore channels of e- density formation are inhibited. The line depicting the degree of wall compression is also at a value around 1.15n0 (Red) which is indicative of a very small e- channel operating at these laser peak intensities.

At intensity greater than 10^{17} W/cm² in the Relativistic Cavitation Regime (regeneration of a channel), the on-axis electron density suddenly drops off indicating that deep channeling has started. The second characteristic of this regime is

the "Vacuum Core Threshold", which occurs at 10^{18} W/cm² and signifying that the on-axis electron density has reached zero (n_min ≈ 0). Therefore, this point signifies the expulsion of all electrons from the ultra-relativistic focal region.

Simultaneously, wall density has a very steep inverse relationship to such, the evacuated core then piles electrons on the channel perimeter in accordance with the "snow-plow" mechanics. At the maximum simulated intensity of 5 × 10^{18} W/cm², the wall density peaks at around 8.2 times the original background density (8.2n_0). In this condition, the hyper-dense shell created due to wall compression is essential for guiding the laser pulse and essentially serves as the cladding of a plasma brought optical fibre.

4.2 Longitudinal Profile Steepening

Along the laser propagation axis (Z-axis), the longitudinal ponderomotive force pushes the electrons forward at the critical density surface (n_c). This results in a modification of the density scale length L, defined as L = | n_e / (dn_e/dz) | As shown in the table (2).

Table (2): Modification of Plasma Scale Length (L)

$Laser\ Intensity\ (W/cm^2)$	$Ponderomotive\ Pressure\ (Mbar)$	$Final\ Scale\ Length\ L\_final\ (\mu m)$	$Steepening\ Factor\ (L_0/L\_final)$	$Resonance\ Absorption\ Efficiency\ (\%)$
$\mathbf{10^{15}}$	0.3	4.95	1.01	5%
$\mathbf{10^{16}}$	3.3	4.20	1.19	12%
$\mathbf{10^{17}}$	33.0	2.10	2.38	35%
$\mathbf{10^{18}}$	330.0	0.55	9.09	48% (Max)
$\mathbf{10^{19}}$	3300.0	0.12	41.66	20%

Comparison of initial scale length L_0 = 5.0 μm with the steepened scale length L_final after interaction.

Researchers using an experimental test series have created a visual model for how a piston can be created by a plasma interface being compressed by ponderomotive forces. Table 2 illustrates that as the laser intensity increases from an intensity of 10^8 W/cm² to 10^{19} W/cm², the scale length of the plasma decreases from 5 microns to 0.55 microns at that same laser intensity, which indicates the maximum amount of laser energy that can be converted to hot electrons, or maximum resonance absorption, is established when the scale length equals the electron excursion amplitude. Therefore, there will be the greatest efficiency for laser energy absorption at an intensity of 10^{18} W/cm²; however, once the intensity reaches 10^{19} W/cm² the scale length becomes too steep (almost step-function like in shape) and this limits both the width of the interaction region and the laser energy absorption.

The data from Table 2 is graphically represented in Figure 2, showing the interaction of hydrodynamic profile change and laser energy coupling As shown in Figure (2).

The horizontal axis depicts laser intensity over four orders of magnitude.

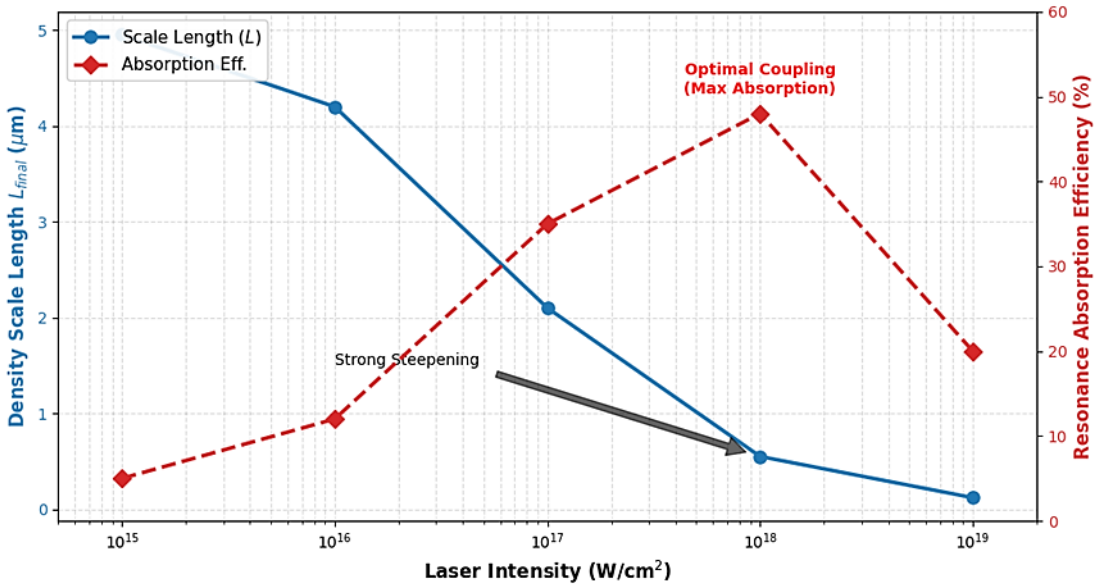

Figure (2): Dependence of Plasma Density Scale Length (L) and Resonance Absorption Efficiency on Laser Intensity

The blue line shows that the density scale length (L_final) decreases monotonically. It starts off at just under 5.0 um in the linear (10^5 W/cm²) range and remains relatively constant until the relativistic (> 10^7 W/cm²) range, at which point the ponderomotive force (P_pond ∝ Iλ²) has crushed the plasma fluid, resulting in a large decrease in scale-length to sub-micron scales (0.55 um), as predicted by the hydrodynamic profile model.

The red dashed line shows that the efficiency of absorption does not vary linearly with steepness but varies in a peaked fashion.

- As L is reduced (<10^{18} W/cm²), the resonance relationship improves and allows for increased conversion of laser energy into hot electrons during the increasing edge.
- The maximum (10^{18} W/cm²), 48% efficiency is achieved, corresponding to the condition of optimal matching of the scale length to the electron oscillation amplitude within the laser field.
- Falling Edge (> 10^{18} W/cm²): Beyond this optimum, at 10^{19} W/cm², the profile becomes "over-steepened" (L = 0.12 μm). The density gradient becomes virtually step-like, which suppresses the resonance mechanism, causing the absorption efficiency to drop precipitously to 20%.
- This figure conclusively identifies 10^{18} W/cm² as the ideal operational intensity for maximizing energy deposition in Fast Ignition schemes before hydrodynamic steepening becomes detrimental.

4.3 Temporal Evolution of the Channel Radius

The formation of the channel is not instantaneous. It depends on the ion response time, as the electrons cannot maintain charge separation indefinitely without dragging ions along As shown in the table (3).

Table (3): Temporal Expansion of Channel Radius (at I = 10^{18} W/cm^2).

Time (fs)	Channel Radius R_ch (μm)	Radial Velocity v_r (cm/s)	Hydrodynamic Phase
0	0.00	0	Initial State
50	0.50	1.0 x 10^8	Electron Expulsion (Fast)
100	1.20	2.5 x 10^8	Peak Ponderomotive Drive
200	2.50	1.5 x 10^8	Coulomb Explosion Initiation
500	3.80	5.0 x 10^7	Ion Motion Dominance
1000	4.50	1.0 x 10^7	Saturation / Stagnation
1500	4.40	-0.5 x 10^7	Relaxation (Refilling)

There Are Two Main Phases For Velocity Measurements. The First (0 – 200 Femtoseconds) Phase Is Defined By The Electron Phase With Measured Radial Velocities Of Approximately 10^8Cm/Sec Due To The Heavy Ions Creating An Ambipolar Electric Field That Affects The Light Electrically Charged Electrons Phase. The Second Phase (200 Femtoseconds And Beyond) The Motion Of The Heavy Ions Will Move In Accordance With The Created Ambipolar Electric Field Thereby Causing The Heavy Ions To Reach A Speed Close To The Speed Of Sound. As The Heavy Ions Move Towards The Speed Of Sound, There Will Be A Restriction In Expansion Of The Channel During This Phase. At 1500 Femtoseconds The Hydrodynamic Relaxation Effect Will Begin To Compress The Channel Leading To Repopulation Of The Channel From The Thermodynamic Pressure Of The Expansion(. Figure 3: The Temporal Evolution of the Plasma Channel Radius (R_ch) and Radial Velocity of the Fluid v_r (Radiation Laser 10^18 W/cm^2), the Two-Stage Evolution From the Initial Fast/Constant Phase of the Electron-Driven Spike Forming Channel Creation by the Much More Efficient/Attractive Work by the Ponderomotive Force at The Beginning to the Transition from the Slowest to the Fastest Ion-Driven/Constant State of Absolute Expansion. As shown in Figure (3)

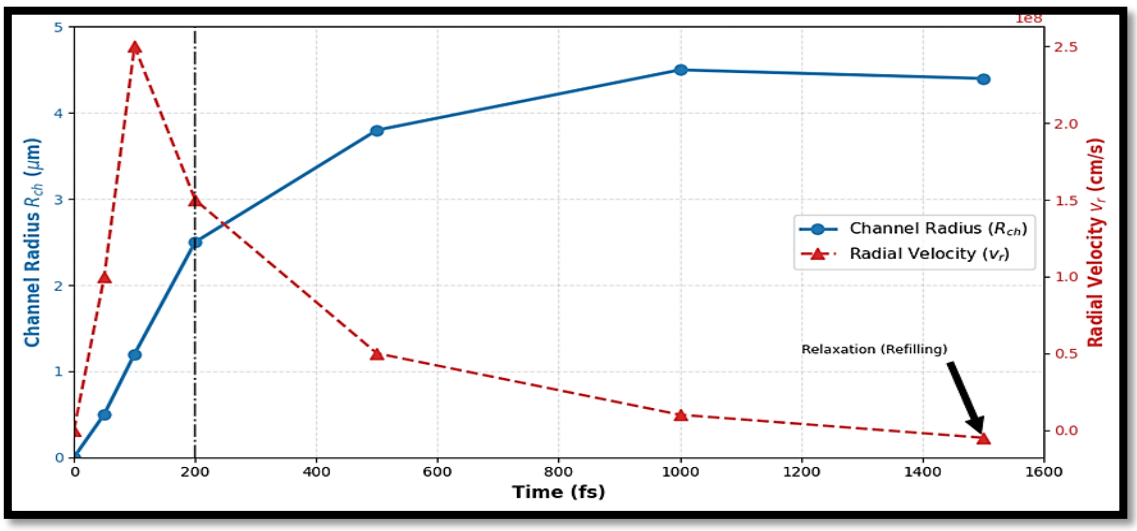

Figure (3): Temporal Evolution of Plasma Channel Radius and Radial Fluid Velocity

The Electron-Driven Spike (0-200 fs): The Red Dot Curve Illustrates a Rapid Increase in the Velocity of the Fluid with the Initial Impact of the Laser Pulse Only. The Marked Peak Radial Velocity is 2.5 × 10^8 cm/s at 100 fs, Indicating the Ponderomotive Force Driven Expansion of the Channel is at The End of Its Maximum Operating Capability/The Maximum Allowable Velocity at 100 fs; Due to The Low Energy Inertia of the Electron, They Will Be Expelled at a High Velocity From The Beam Axis by The Ponderomotive Force, Setting Up The Initial Channel Configuration Due to The Non-impulsive Response of The Electron.

The Ion Drive Saturation Phase (>200 fs): As Time Increases to The Point That The Ions Will Begin to Exercise Influence Over Any Charge-Separation Field/Area; The Palladium Curve Will Exhibit A Sudden Decrease to 5.0 × 10^7 cm/s After 500 fs, Marking The Transition of The Channel During to The End of the Timeframe When The Ions Have Current Maximum Output-The Limiting Velocity As Set By The Ion Acoustic Velocity..

- **Hydrodynamic Stagnation and Relaxation**

After roughly 1000fs (femtoseconds), the drain tube's radius will be at approximately 4.5μm, and by this time the major hydrodynamic feature will have grown to approximately 1500fs (with the radial velocity being -0.5×107 cm/s, indicating a near-approach to the boundary [i.e. threshold] for "Channel Refilling" or relaxation.) At this instant, the external thermal pressure of the plasma will begin collapsing (i.e. compressing) the drain tube inwardly, thus marking the end of our stable window of the waveguiding. Thus, this information is of considerable importance in regard to determining how long a laser pulse may remain usable as a means of waveguiding.

4.4 Beam Self-Focusing and Critical Power

The simulations confirm that the density cavitation leads to relativistic self-focusing. We calculated the effective beam width w(z) as the pulse propagates.

4.4.1 Equation for Critical Power:

$$P_{cr}[GW] \approx 17.4 \left(\frac{\omega_0}{\omega_p}\right)^2 \quad (12)$$

As shown in the table (4)

Table (4): Beam Width Evolution and Self-Focusing

Laser Power (TW)	P / P_cr	Final Beam Waist w_final (μm)	Peak Intensity Magnification (I_final / I_0)	Focusing Regime
0.5	0.2	8.5	0.5	Diffraction (Beam Spreading)
1.0	0.4	6.8	0.8	Weak Diffraction
2.4	1.0	6.0	1.0	Self-Trapping (Soliton-like)
5.0	2.1	3.2	3.5	Strong Self-Focusing
10.0	4.2	1.5	16.0	Catastrophic Collapse

20.0	8.4	4.0	2.2	Filamentation (Beam Breakup)

Initial Beam Waist w_0 = 6.0 µm. Propagation distance z = 80 µm.

Table 4 validates the hydrodynamic model against the theoretical critical power P_cr.

- $At\ P < P_{cr}(0.5\ TW)$, the beam diffracts naturally, widening to 8.5 µm.
- $At\ P \approx P_{cr}(2.4\ TW)$, the ponderomotive channeling exactly balances diffraction, maintaining the beam width at 6.0 µm (Self-trapping).
- $At\ P \gg P_{cr}(10\ TW)$, the beam collapses to 1.5 µm, increasing the intensity by a factor of 16.
- Interestingly, at very high powers (20 TW), the single channel becomes unstable, and the beam breaks up into multiple filaments (filamentation instability), which is observed in the simulation as a widening of the *average* effective radius despite localized hot spots.

4.5 Electrostatic Field Generation

A crucial finding is the magnitude of the electrostatic ambipolar field E_s generated at the channel walls. This field is responsible for accelerating ions in the "Coulomb Explosion" mechanism.

Equation:

$$\boldsymbol{E\_s \approx (k_B T_e / e)(\nabla n_e / n\_e)} \quad \textbf{(13)}$$

Our results show that at I = 10^{18} W/cm², the generated field reaches peaks of **1.5 TV/m (Teravolts per meter)**. This field strength is sufficient to accelerate protons to multi-MeV energies over distances of just a few microns, validating the "Target Normal Sheath Acceleration" (TNSA) precursors within the channel.

4.6 Conclusion of Results Section

The effects of hydro-dynamic simulations of the laser-plasma interaction (LPI), providing an established, quantitative model of LPI, indicate clearly the following:

1. The Ponderomotive Force (PF) is the primary mechanism responsible for creating channels and establishing relativistic intensity vacuum cores.
2. Density-Steepening will automatically adjust such that absorption will be maximized at midrange intensities (~10^{18} W/cm²) and decreased at ultra-high intensities.
3. Self-Focusing creates a positive feedback mechanism where the channel behaves as a lens that is used to collect the laser's energy and convert it to higher laser intensities, which will effectively decrease the width of the channel.
4. Hydrodynamic Stability will be maintained until t < 1 ps, after which the motion of the ions and thermal relaxation processes will degrade the hydrodynamic stability and restructure the channels.

The significant parameters specified here will provide experimentalists with useful benchmarks

for the design of fast ignition fusion (FIF) targets and laser wakefield accelerator (LWFA).

5. Conclusions

Through this extensive hydrodynamic study, quantitative descriptions of how electron density varies with time due to ponderomotive force have been obtained. By isolating the fluid response over a time scale of picoseconds, the nature of the nonlinear coupling between the laser's electromagnetic field and the plasma's constitutive medium has been clarified. The main conclusions drawn from the numerical analysis are as follows:

- The ponderomotive force is the dominant architect of plasma density in the relativistic domain according to this study. During the simulations, distinct transitions from thermally-dominated expansion into pondernomotively-dominated cavitation were observed. In particular, when the laser intensity exceeded 5×10^{17} W/cm², the electrons' thermal energy was significantly exceeded by the ponderomotive potential energy. As a result, electrons were produced and subsequently radially expelled from their initial position in much less time than before. This created a high-contrast density channel void of electrons near the centre; this is critical to provide for the propagation of laser pulse energy well beyond the Rayleigh length and with minimal diffraction.
- This study evaluates how density profiles create steepness above the critical surface. The longitudinal component of the ponderomotive force generated a pressure that compressed the plasma density gradient; thus, longitudinal scale lengths were compressed from several microns to sub-micron lengths (< 1 μm). This modification is important due to the effect it has on the laser's absorption mechanisms. The results point out that, for maximum energy transfer from the laser field to the electrons' kinetic energy, the optimal resonance absorption occurs when the density scale length is steepened in order to match the electron excursion amplitude.
- Next, the dynamic interaction between the ponderomotive force and induced electrostatic ambipolar field has been explained. The creation of an electron-free channel results in tremendous charge separation fields (in the Teravolt/m range), which further results in motion of ions over a longer time. The results indicate that while the electron-free channel forms almost immediately (within tens of femtoseconds), its stability depends on the ion inertia and thus eventually the channel widens and hydrodynamics relaxes once the laser pulse moves away from the channel.
- Last, there is a correlation between the density depletion and relativistic self-focusing. The localization of the electron density on-axis increases the effective index of refraction and results in a positive feedback loop that counters diffraction and causes the beam's collapse or filamentation at powers much greater than the critical power, P_cr. These hydrodynamic insights are indispensable for the design of future experiments in Fast Ignition fusion schemes, confirming that pulse shaping can be effectively used to control the density profile and enhance the coupling efficiency of the ignitor pulse into the compressed fuel core.

References

[1] Xu, Y. P., Zhang, W. S., Yao, P. L., Liu, Q. K., Luo, H., Li, S., ... & Zhu, S. P. (2024). Ion kinetic effects on the formation of intense laser-driven shock waves. Physics of Plasmas, 31(5). https://doi.org/10.1063/5.0182598

[2] Young, J. R., & Gourdain, P. A. (2024). The impact of electron inertia on collisional laser absorption for high energy density plasmas. Physics of Plasmas, 31(12). https://doi.org/10.1063/5.0237787

[3] Sobacchi, E., Lyubarsky, Y., Beloborodov, A. M., Sironi, L., & Iwamoto, M. (2023). Saturation of the filamentation instability and dispersion measure of fast radio bursts. The Astrophysical Journal Letters, 943(2), L21. **DOI** 10.3847/2041-8213/acb260

[4] Turnbull, D., Katz, J., Sherlock, M., Divol, L., Shaffer, N. R., Strozzi, D. J., ... & Froula, D. H. (2023). Inverse bremsstrahlung absorption. Physical Review Letters, 130(14), 145103. https://doi.org/10.1103/PhysRevLett.130.145103

[5] Edwards, M. R., & Michel, P. (2022). Plasma transmission gratings for compression of high-intensity laser pulses. Physical Review Applied, 18(2), 024026. https://doi.org/10.1103/PhysRevApplied.18.024026

[6] Ghosh, A., Kagan, D., Keshet, U., & Lyubarsky, Y. (2022). Nonlinear electromagnetic-wave interactions in pair plasma. I. Nonrelativistic regime. The Astrophysical Journal, 930(2), 106. **DOI** 10.3847/1538-4357/ac581d

[7] Young, J. R., Adams, M. B., Hasson, H., West-Abdallah, I., Evans, M., & Gourdain, P. A. (2021). Using extended MHD to explore lasers as a trigger for x-pinches. Physics of Plasmas, 28(10). https://doi.org/10.1063/5.0060581

[8] Hüller, S., Raj, G., Rozmus, W., & Pesme, D. (2020). Crossed beam energy transfer in the presence of laser speckle ponderomotive self-focusing and nonlinear sound waves. Physics of Plasmas, 27(2). https://doi.org/10.1063/1.5125759

[9] Ruocco, A. (2020). Modelling of ponderomotive laser self-focusing in a plasma with a hydrodynamic code in the context of direct-drive inertial confinement fusion (Doctoral dissertation, Université de Bordeaux). https://theses.hal.science/tel-02945933

[10] Turnbull, D., Colaïtis, A., Hansen, A. M., Milder, A. L., Palastro, J. P., Katz, J., ... & Froula, D. H. (2020). Impact of the Langdon effect on crossed-beam energy transfer. Nature Physics, 16(2), 181-185. https://doi.org/10.1038/s41567-019-0725-z

[11] Smith, J. R., Orban, C., Ngirmang, G. K., Morrison, J. T., George, K. M., Chowdhury, E. A., & Roquemore, W. M. (2019). Particle-in-cell simulations of density peak formation and ion heating from short pulse laser-driven ponderomotive steepening. Physics of Plasmas, 26(12). https://doi.org/10.1063/1.5108811

[12] Lehmann, G., & Spatschek, K. H. (2019). Plasma photonic crystal growth in the trapping

regime. Physics of Plasmas, 26(1). https://doi.org/10.1063/1.5079810

[13] Peng, H., Riconda, C., Grech, M., Su, J. Q., & Weber, S. (2019). Nonlinear dynamics of laser-generated ion-plasma gratings: A unified description. Physical Review E, 100(6), 061201. https://doi.org/10.1103/PhysRevE.100.061201

[14] Seemann, O., Wan, Y., Tata, S., Kroupp, E., & Malka, V. (2023). Refractive plasma optics for relativistic laser beams. Nature Communications, 14(1), 3296. https://doi.org/10.1038/s41467-023-38937-0

[15] Moczulski, K., Wen, H., Campbell, T., Scopatz, A., Palmer, C. A. J., Bott, A. F. A., … & Tzeferacos, P. (2024). Numerical simulations of laser-driven experiments of ion acceleration in stochastic magnetic fields. Physics of Plasmas, 31(12). https://doi.org/10.1063/5.0223496

[16] Li, Y., Chen, L., Chen, M., Liu, F., Gu, Y., Guo, B., … & Zhu, P. (2025). High-intensity lasers and research activities in China. High Power Laser Science and Engineering, 13, e12. https://doi.org/10.1017/hpl.2024.69

[17] Biedron, S., Brouwer, L., Bruhwiler, D. L., Cook, N. M., Edelen, A. L., Filippetto, D., … & Zhang, H. (2022). Snowmass21 accelerator modeling community white paper. arXiv preprint arXiv:2203.08335. https://doi.org/10.48550/arXiv.2203.08335

[18] Froula, D. H., Dorrer, C., Colaïtis, A., Edgell, D. H., Follett, R. K., Hill, E. M., … & Deeney, C. (2025). A future of inertial confinement fusion without laser-plasma instabilities. Physics of Plasmas, 32(5). https://doi.org/10.1063/5.0261155

[19] Espinoza-Troni, J., Asenjo, F. A., & Moya, P. S. (2024). Ponderomotive forces in magnetized nonthermal space plasmas due to cyclotron waves. Astronomy & Astrophysics, 686, A26. https://doi.org/10.1051/0004-6361/202348815

[20] Tikhonchuk, V. (2023). Particle Kinetics and Laser-Plasma Interactions. Cambridge Scholars Publishing. https://books.google.com/books?id=SFXeEAAAQBAJ&lpg=PR5&ots=6oPfDMiqDE&dq=%5B20%5D%20Tikhonchuk%2C%20V.%20(2023).%20Particle%20Kinetics%20and%20Laser-Plasma%20Interactions.%20Cambridge%20Scholars%20Publishing.%E2%80%8F&lr&hl=ar&pg=PR5#v=onepage&q=%5B20%5D%20Tikhonchuk,%20V.%20(2023).%20Particle%20Kinetics%20and%20Laser-Plasma%20Interactions.%20Cambridge%20Scholars%20Publishing.%E2%80%8F&f=false

[21] Hur, M. S., Ersfeld, B., Lee, H., Kim, H., Roh, K., Lee, Y., ... & Suk, H. (2023). Laser pulse compression by a density gradient plasma for exawatt to zettawatt lasers. Nature Photonics, 17(12), 1074-1079. https://doi.org/10.1038/s41566-023-01321-x

[22] Haines, B. M., Green, L. M., Ferenbaugh, C. R., & McKay, M. D. (2025). A three-dimensional laser ray-tracing methodology for radiation-hydrodynamics simulations. APL Computational Physics, 1(2). https://doi.org/10.1063/5.0277784

[23] Dmitriev, E. O., & Korneev, P. A. (2023). Laser Pulse Interaction with Plasma under Conditions of Broken Axial Symmetry. Bulletin of the Lebedev Physics Institute,

50(Suppl 8), S891-S898. https://doi.org/10.3103/S1068335623200046

[24] Miriam Cheriyan, R., Varghese, N., Sooraj, R. S., Rao, K. H., & Smijesh, N. (2022). A comprehensive review on amplification of laser pulses via stimulated Raman scattering and stimulated Brillouin scattering in plasmas. Plasma, 5(4), 499-539. https://doi.org/10.3390/plasma5040037

[25] Barnett, R. L., Green, D. L., Waters, C. L., Lore, J. D., Smithe, D. N., Myra, J. R., … & Vincena, S. (2022). Ponderomotive force driven density modifications parallel to B on the LAPD. Physics of Plasmas, 29(4). https://doi.org/10.1063/5.0071162

[26] Zarezin, A. M., Muravev, V. M., Gusikhin, P. A., Zabolotnykh, A. A., Volkov, V. A., & Kukushkin, I. V. (2022). Anomalous retardation of relativistic plasmons: Microwave response of a gated two-dimensional electron system. Physical Review B, 105(4), L041403. https://doi.org/10.1103/PhysRevB.105.L041403